

Multi-component magneto-optical conductivity of multilayer graphene on SiC

I. Crassee¹, J. Levallois¹, D. van der Marel¹, A. L. Walter^{2,3}, Th. Seyller⁴ and A. B. Kuzmenko¹

¹*Département de Physique de la Matière Condensée,
Université de Genève, CH-1211 Genève 4, Switzerland*

²*Dept. of Molecular Physics,
Fritz-Haber-Institut der Max-Planck-Gesellschaft,
Faradayweg 4-6, 14195 Berlin, Germany*

³*E. O. Lawrence Berkeley National Laboratory,
Advanced Light Source, MS6-2100, Berkeley, CA 94720*

⁴*Lehrstuhl für Technische Physik,
Universität Erlangen-Nürnberg,
Erwin-Rommel-Str. 1, 91058 Erlangen, Germany*

(Dated: December 13, 2021)

Far-infrared diagonal and Hall conductivities of multilayer epitaxial graphene on the C-face of SiC were measured using magneto-optical absorption and Faraday rotation in magnetic fields up to 7 T and temperatures between 5 and 300 K. Multiple components are identified in the spectra, which include: (i) a quasi-classical cyclotron resonance (CR), originating from the highly doped graphene layer closest to SiC, (ii) transitions between low-index Landau levels (LLs), which stem from weakly doped layers and (iii) a broad optical absorption background. Electron and hole type LL transitions are optically distinguished and shown to coexist. An electron-hole asymmetry of the Fermi velocity of about 2% was found within one graphene layer, while the Fermi velocity varies by about 10% across the layers. The optical intensity of the LL transitions is several times smaller than what is theoretically expected for isolated graphene monolayers without electron-electron and electron-phonon interactions.

I. INTRODUCTION

Graphene attracts much interest due to the intriguing physical properties and a potential for novel applications. Epitaxially grown graphene on SiC¹ is particularly promising for large-scale production. The growth conditions of epitaxial graphene were constantly improving in the last years, which resulted in a macroscopic continuity of graphene layers and an enhanced mobility of charge carriers¹⁻⁶. Electronic properties of epitaxial graphene grown on Si- and C-faces of SiC, are markedly different^{7,8}. Interestingly, multilayer epitaxial graphene produced on the carbon face shows a number of electronic features typical of isolated monolayer graphene as revealed by infrared spectroscopy⁹, scanning tunneling microscopy (STM)^{10,11}, angle-resolved photoemission spectroscopy (ARPES)¹² and quantum Hall effect¹³. In particular, the Landau levels in this material demonstrate a square-root dependence on the perpendicular magnetic field B and the level index $n(= 0, \pm 1, \dots)$:

$$E_n = E_D + \text{sgn}(n) \sqrt{2e\hbar v_F^2 |nB|}, \quad (1)$$

where v_F is the Fermi velocity and E_D is the Dirac-point energy. It is generally believed that such an effective electronic interlayer decoupling is a result of twisted, non-Bernal stacking of the C-face grown graphene layers. Significant progress in theoretical understanding of

the influence of stacking on the electronic structure and Landau levels was made¹⁴⁻²². However, no complete theory able to quantitatively predict the effect of twisting on the band structure at an arbitrary stacking angle exists at the moment even for bilayer graphene. In real samples, many layers are present with a random rotation between each pair of neighbors. Moreover, the substrate induces a strong variation of the Dirac-point energy E_D with respect to the chemical potential and therefore a very different density and mobility of carriers in different layers. More experiments are needed to understand the complex electronic structure of this system and establish favorable conditions for applications.

Infrared spectroscopy, which is a direct probe of charge dynamics, is well suited to study carriers in graphene. Optical spectra contain contributions from all graphene layers, including those that are not seen by surface probes, such as ARPES and STM. In a recent work²³, we measured the rotation of polarization of light passing through epitaxial graphene in a magnetic field, known as the Faraday effect. Being an optical analogue to the d.c. Hall effect, the Faraday rotation reveals the sign of the charge carriers involved in various LL transitions. Moreover, optical spectroscopy allows separating carriers by their high-frequency dynamics, in contrast to the d.c. transport measurements. Here we present an extensive magneto-optical study of multilayer epitaxial graphene grown on the carbon side of SiC, by combining the Faraday rotation measurements with the transmission spectra

and extracting both the diagonal and Hall optical conductivity. Different magneto-optical contributions are disentangled and studied quantitatively using a multi-component CR model. This approach reveals a number of interesting properties of multiple charge carriers in multilayer graphene, for example, the simultaneous presence of both electron- and hole-like components as well as the existence of carriers with different Fermi velocities. It also allows us to analyze optical intensities of various transitions and make comparison to theoretical models. Finally, the dependence of optical spectra on temperature and environmental (surface) doping are studied.

II. TECHNIQUES

The rotationally stacked multilayer graphene on the carbon terminated side of 6H-SiC was produced by hydrogen etching at 1450°C and subsequent graphitization in an argon atmosphere at 1650°C. The substrate has a thickness of 370 μm and a surface area of $10 \times 10 \text{ mm}^2$. The back side of the substrate was cleaned from undesirably grown graphene using scotch tape. Using X-ray photoemission spectroscopy we estimated the number of graphene layers to be 5 ± 1 and checked that the backside is graphene free. Additionally, we performed mid-infrared transmission microscopy over an area comparable to the total area used for the magneto-optical experiment using a spot size of $10 \times 10 \mu\text{m}^2$. We assume that each graphene layer absorbs 1.5% of light at 1 eV, which is the value expected for monolayer graphene on SiC, provided that the chemical potential does not exceed 0.5 eV. This absorption value is lower than the absorption of 2.3% of free-standing graphene, because the refractive index of SiC is larger than 1. The infrared absorption shows a distribution peaked at 7 layers with a FWHM of 2.7 layers. The slightly larger number of layers revealed by infrared microscopy can be related to an underestimation of the absorption of one layer. Notably, both measurements show that at least 4 layers are present at any point of the sample.

We measured the Faraday rotation $\theta(\omega)$ and magneto-optical transmission $T(\omega)$ in the range of photon energies $\hbar\omega$ between 8 and 80 meV as described in Ref. 23. The optical transmission was measured with respect to a bare SiC substrate without graphene, which underwent similar hydrogen etching at 1450°C as the graphitized sample. The optical spot had a diameter of 5 mm. Two series of measurements were performed: first by varying temperature between 5 and 300 K at a fixed magnetic field of 3 T and then by varying magnetic field from 0 to 7 T at a constant temperature of 5 K. Within each series, the optical absorption and the Faraday rotation were measured one after another with a shortest possible delay. During the experiments the sample was in a He gas flow; between the production and the experiments, as well as between the first and second series, it was stored in desiccated

air. As will be shown later, even these precautions did not allow us to completely avoid surface contamination, which has an effect on charge dynamics in the top layers. Therefore, the data presented in this paper differ somewhat from data presented in Ref.²³, although the same sample was used.

The real parts of the diagonal, $\sigma_{xx}(\omega)$, and Hall, $\sigma_{xy}(\omega)$, optical conductivities can be directly obtained from the magneto-optical absorption and Faraday rotation by using the general thin-film approximation, taking internal reflections in the substrate into account:

$$1 - T(\omega) \approx 2Z_0 f_s(\omega) \text{Re}[\sigma_{xx}(\omega)] \quad (2)$$

$$\theta(\omega) \approx Z_0 f_s(\omega) \text{Re}[\sigma_{xy}(\omega)] \quad (3)$$

where $Z_0 \approx 377 \Omega$ is the impedance of vacuum and $f_s(\omega)$ is a spectrally smooth dimensionless function specific to the substrate²³. These relations are obtained by linear expansion of the exact Fresnel formulas, which is accurate for our sample with only a few graphene layers. We reduced the spectral resolution to 1 meV in order to suppress the Fabry-Perot interference in the substrate. In this case:

$$f_s(\omega) = \frac{1}{n_s + 1} + \frac{2n_s}{n_s^2 - 1} \cdot \frac{q^2}{1 - q^2} \quad (4)$$

where $q = [(n_s - 1)/(n_s + 1)]^2 \exp[-(2\omega/c)k_s d]$, d , $n_s(\omega)$ and $k_s(\omega)$ are the thickness, the refractive index and extinction coefficient of the substrate. The latter quantities, which are independent of magnetic field, were determined from measurements of the absolute transmission and reflection spectra of the bare SiC at every used temperature.

The complex magneto-optical conductivity tensor:

$$\hat{\sigma}(\omega) = \begin{bmatrix} \sigma_{xx}(\omega) & \sigma_{xy}(\omega) \\ -\sigma_{xy}(\omega) & \sigma_{xx}(\omega) \end{bmatrix} \quad (5)$$

is diagonal in the circular basis $\vec{x} \pm i\vec{y}$, with eigenvalues:

$$\sigma_{\pm}(\omega) = \sigma_{xx}(\omega) \pm i\sigma_{xy}(\omega). \quad (6)$$

The absorption of right- and left-handed circular polarizations (which are shown in the insets of Fig.1c and 1d) is described by the real parts of $\sigma_{+}(\omega)$ and $\sigma_{-}(\omega)$ respectively. This basis provides an intuitive way to present the magneto-optical conductivity showing individual LL transitions, which are active for strictly one circular polarization or the other²⁴⁻²⁶. In particular, for right circularly polarized light, transitions between electron like LLs with $n \geq 0$, such as $\text{LL}_{0 \rightarrow 1}$, $\text{LL}_{1 \rightarrow 2}$ etc, are active, provided that the chemical potential is in between the corresponding LLs (the symbol $\text{LL}_{i \rightarrow j}$ is used to designate the LL transition between levels i and j). Similarly, for left circularly polarized light, transitions between hole like LLs, ($\text{LL}_{-1 \rightarrow 0}$, $\text{LL}_{-2 \rightarrow -1}$, etc.) are excited²⁷.

From Eq. (6) one can see that the imaginary part of $\sigma_{xy}(\omega)$ is needed to obtain the real part of the magneto-optical conductivity in the circular basis. Experimentally, $\text{Im}[\sigma_{xy}(\omega)]$ is directly related to the ellipticity of

the transmitted light. However, in the present experiment the error bars on the ellipticity are larger than the ones on the Faraday angle. Therefore, instead of directly applying Eq. (6) to the experimental data, we plot $\sigma_{\pm}(\omega)$ obtained from the results of the multi-component fitting discussed in Section III A. For simplicity, in the rest of the paper, the symbols σ_{xx} , σ_{xy} , σ_+ and σ_- will be used to denote the real parts of the corresponding complex functions, unless stated otherwise.

III. RESULTS

A. Magneto-optical conductivity at 3 T and 5 K

Figure 1 shows representative conductivity spectra at $B = 3$ T and $T = 5$ K. The diagonal and Hall conductivities are plotted as solid lines in Fig. 1a and 1b. They are expressed in dimensionless units of $\sigma_0 = e^2/4\hbar$, which is equal to the universal optical conductivity of monolayer graphene²⁸. The rich structure of the spectra indicates the presence of multiple optical transitions. The absorption at low energy, shown by the arrow, corresponds to quasi-classical CR coming from the highly doped graphene layer closest to the SiC substrate²³. At about 60 to 70 meV, a strong peak in $\sigma_{xx}(\omega)$ is observed that matches the energy of the $LL_{0\rightarrow 1}$ or $LL_{-1\rightarrow 0}$ transitions at this field. The Hall conductivity displays a ‘zig-zag’ shape in this spectral range, suggesting that there are multiple components contributing to the optical response. In addition, a structure is present at about 27 meV, most clearly seen in $\sigma_{xy}(\omega)$, resulting from the $LL_{1\rightarrow 2}$ transition.

In order to disentangle different contributions to the magneto-optical spectra we used a multi-component model where the total conductivity is given by a sum of separate cyclotron resonances. In the circular basis the total complex magneto-optical response is given by:

$$\sigma_{\pm}(\omega) = \sum_j \frac{2W_j}{\pi} \cdot \frac{i}{\omega \mp \omega_{c,j} + i\gamma_j} \quad (7)$$

and the complex diagonal and Hall optical conductivities are accordingly expressed by:

$$\sigma_{xx}(\omega) = \sum_j \frac{2W_j}{\pi} \cdot \frac{\gamma_j - i\omega}{\omega_{c,j}^2 - (\omega + i\gamma_j)^2} \quad (8)$$

$$\sigma_{xy}(\omega) = \sum_j \frac{2W_j}{\pi} \cdot \frac{-\omega_{c,j}}{\omega_{c,j}^2 - (\omega + i\gamma_j)^2}, \quad (9)$$

where $\omega_{c,j}$ is the cyclotron frequency, W_j is the spectral weight and γ_j is the broadening of the j th component. Physically speaking, each component can describe either a quasi-classical CR or a transition between individual LLs separated by energy $|\hbar\omega_{c,j}|$. Notably, $\sigma_{xx}(\omega)$ does not depend on the sign of the charge carriers, unlike $\sigma_{xy}(\omega)$, where the sign can be derived directly from the spectral shape²³. In $\sigma_{xx}(\omega)$ each component results in

a peak centered at $|\omega_{c,j}|$. In $\sigma_{xy}(\omega)$ however, it shows an antisymmetric structure, where $|\omega_{c,j}|$ corresponds to the inflection point in the curve. The slope at this point coincides with the sign of the cyclotron frequency and reveals the polarity of the charge carriers involved in the transition²³. In particular, a positive (negative) slope signals electron (hole) like carriers.

The spectra $\sigma_{xx}(\omega)$ and $\sigma_{xy}(\omega)$ were simultaneously fitted using Eqs. (8) and (9), while allowing the parameters $\omega_{c,j}$, W_j and γ_j to change freely. The fitting curves are shown in Fig. 1a and 1b, as black dotted lines. We found that a minimal model describing satisfactorily the spectral structures contains six components, which are shown separately in the same panels.

Interestingly, it was necessary to introduce at least three components with transition energies between 60 meV and 70 meV to describe the structure in this range. Two of the resonances are electron like, which we designate as $LL_{0\rightarrow 1,a}$ and $LL_{0\rightarrow 1,b}$, and one is hole like, referred to as $LL_{-1\rightarrow 0}$. Note that all these transitions are actually at different energies, which is clearly seen already from the presence of three inflection points in the optical Hall conductivity. A fourth component is at about 27 meV and corresponds to the electron like $LL_{1\rightarrow 2}$ transition. The fifth component with a small value of $\hbar\omega_c = 9$ meV originates from a quasi-classical electron like CR. Finally, there is a component with zero cyclotron frequency and large scattering, which forms a broad absorption background present in $\sigma_{xx}(\omega)$, but absent in $\sigma_{xy}(\omega)$. A possible origin of this background will be discussed in Section IV.

The different contributions from electrons and holes to the magneto-optical conductivity are easily seen in the basis of circularly polarized light as shown in Fig. 1c and 1d. The electron like transitions $LL_{0\rightarrow 1,a}$, $LL_{0\rightarrow 1,b}$, $LL_{1\rightarrow 2}$ as well as the CR show peaks in $\sigma_+(\omega)$, while the hole like $LL_{-1\rightarrow 0}$ transition manifests itself in $\sigma_-(\omega)$. Because of the small value of ω_c and a relatively large scattering, the CR component has also a tail in $\sigma_-(\omega)$. The absorption background contributes equally to $\sigma_+(\omega)$ and $\sigma_-(\omega)$.

B. Dependence on magnetic field

The magnetic field dependence of $\sigma_{xx}(\omega)$ and $\sigma_{xy}(\omega)$, measured at 5 K, is shown in Fig. 2a and 2b. The multi-component character of the spectra is present at different fields, although the resonances show a strong field dependence. The model described in Section III A was used to fit $\sigma_{xx}(\omega)$ and $\sigma_{xy}(\omega)$ simultaneously for every field. The fits, shown as black dotted lines, are used to calculate the magneto-optical conductivities in the basis of right and left handed circularly polarized light according to Eq. (7), which are plotted in Fig. 2c and 2d.

The field dependence of all fitting parameters is shown in Fig. 3. The energy of the CR is linear in field, as seen in Fig. 3a. This quasi-classical behavior is expected for

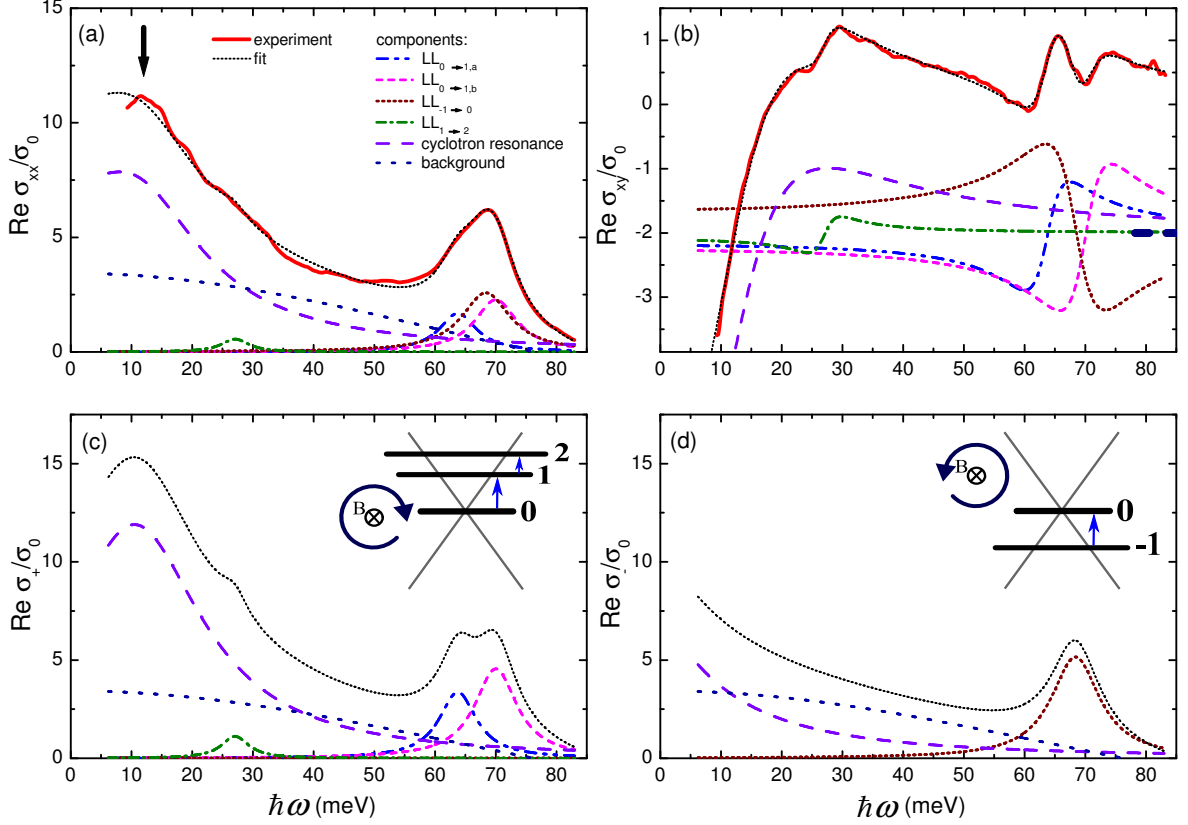


FIG. 1. The diagonal (a) and Hall (b) optical conductivity at 3 T and 5 K, normalized to the universal conductivity σ_0 , and results of the multi-component modeling described in the text. The components in the graph are the individual contributions needed to create the total fit shown by the black dotted line on top of the data. The components in panel (b) have an offset indicated by the blue dashed line at the right side of the graph. Panels (c) and (d): the optical conductivities in the circular basis $\sigma_+(\omega)$ and $\sigma_-(\omega)$ corresponding to the absorption of right and left circular polarized light respectively. In the insets the low-index LL transitions allowed in the corresponding polarizations are shown.

highly doped graphene, where large-index LLs are close to the Fermi energy^{28,29}. In this case the quasi-classical cyclotron frequency is inversely proportional to the Fermi energy ϵ_F :

$$\omega_c = \frac{|e|Bv_F^2}{\epsilon_F}. \quad (10)$$

Using this relation and taking as an estimate $v_F = 1.0 \times 10^6$ m/s we obtain $\epsilon_F = 0.24$ eV, which corresponds to a carrier concentration $n = \epsilon_F^2 / \pi v_F^2 \hbar^2 = 4.2 \times 10^{12}$ cm⁻².

The spectral weight W of the cyclotron peak, shown in Fig. 3d, is field independent within the experimental accuracy. In the absence of interactions, the Drude weight in a single graphene layer is related to ϵ_F by the formula:

$$\frac{\hbar W}{\sigma_0} = 2|\epsilon_F|. \quad (11)$$

This gives $\epsilon_F = 0.16$ eV and accordingly $n = 1.9 \times 10^{12}$ cm⁻², which are significantly smaller than the values

based on the cyclotron frequency. It is possible that interactions renormalize the Drude weight and spread the missing weight over a large spectral range. In our fits this missing weight might be ‘absorbed’ by the broad background component mentioned above. On the other hand, we obtain a reduced Drude weight based on the assumption that for the bottom layer $v_F = 1.0 \times 10^6$ m/s. Accepting a smaller Fermi velocity (by about 20%) would make the cyclotron resonance and the Drude weight match according to Eqs. (10) and (11).

The scattering rate $\hbar\gamma$ (Fig. 3g) of the cyclotron peak is field independent and equal to about 14 meV. Using the semi-classical relation:

$$\mu = \frac{|\omega_c|}{\gamma|B|} \quad (12)$$

we find a mobility of about 2000 cm²/Vs, based on the experimental values of the scattering rate and the cyclotron frequency. Magneto-transport measurements show that the carrier density and mobility in multilayer graphene are correlated³⁰. The values of n and μ that we obtain

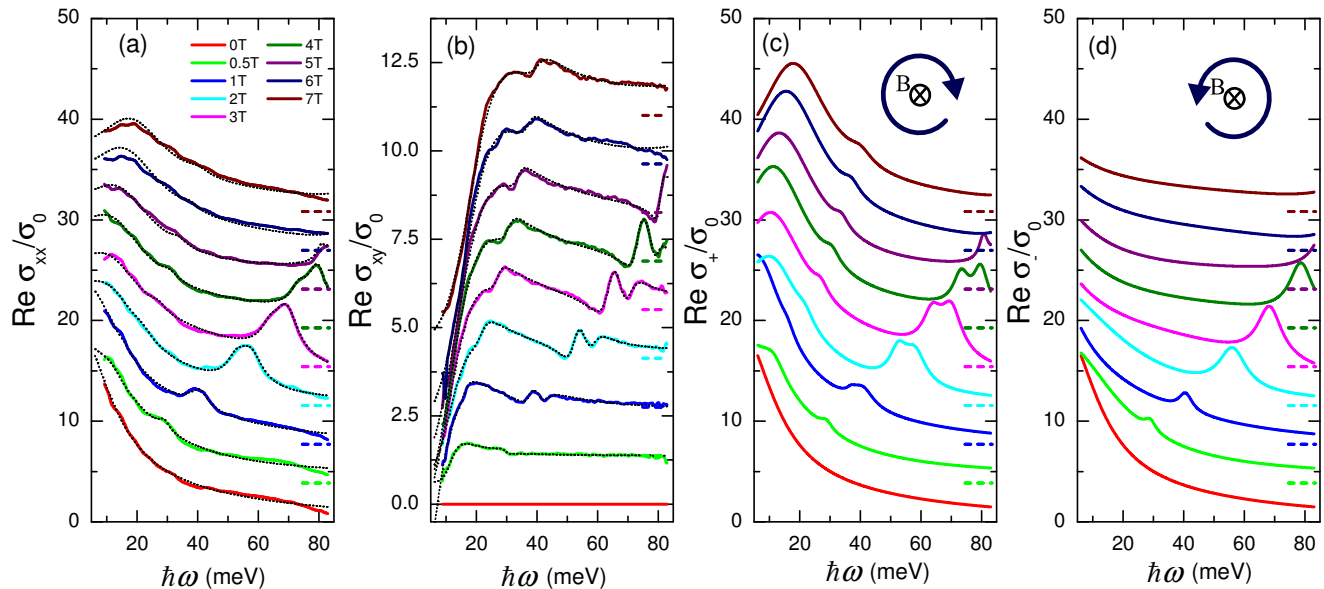


FIG. 2. Magneto-optical conductivity of multilayer graphene at 5 K, normalized to the universal conductivity σ_0 , for several magnetic fields up to 7 T. The curves in all panels are offset as indicated by the dashed lines. Larger offsets correspond to higher magnetic fields. Panels (a) and (b) show the measured spectra of $\sigma_{xx}(\omega)$ and $\sigma_{xy}(\omega)$ (solid lines) and multi-component fits (black dotted lines). In panels (c) and (d) the model-derived $\sigma_+(\omega)$ and $\sigma_-(\omega)$ are shown.

Transition	v_F (m/s)
$LL_{0 \rightarrow 1,a}$	1.02×10^6
$LL_{0 \rightarrow 1,b}$	1.11×10^6
$LL_{-1 \rightarrow 0}$	1.09×10^6
$LL_{1 \rightarrow 2}$	1.01×10^6

TABLE I. Fermi velocities found for different LL transitions.

here for the CR fall on the generic dependence found in Ref. 30. CR was also observed in monolayer epitaxial graphene on the silicon side of silicon carbide^{23,31}, where similar mobility of carriers was found²³.

Next we discuss the field dependence of the LL transitions. From $\sigma_+(\omega)$ and $\sigma_-(\omega)$ it is particularly evident that the two electron like and one hole like resonances described above have a similar magnetic field dependence. The energies of all low-index LL transitions, namely $LL_{1 \rightarrow 2}$ (Fig. 3a), $LL_{0 \rightarrow 1,a}$, $LL_{0 \rightarrow 1,b}$ and $LL_{-1 \rightarrow 0}$ (Fig. 3b), clearly follow the square-root dependence on magnetic field typical of massless Dirac fermions (Eq. (1)), in accordance with previous observations in similar epitaxial graphene samples⁹ and exfoliated monolayer flakes^{32,33}. Fitting the field dependence of the LL transition energies using Eq. (1) provides the Fermi velocities listed in Table I; they show a spread of about 10%. The difference between the Fermi velocities found from the electron like $LL_{0 \rightarrow 1,b}$ and hole like $LL_{-1 \rightarrow 0}$ transitions is only about 2%. However, the presence of three distinct inflection points in $\sigma_{xy}(\omega)$ corresponding to the energies of the three LL transitions, is a clear sign that the transition energies and therefore the Fermi velocities are different.

The spectral weights of the $LL_{1 \rightarrow 2}$, $LL_{0 \rightarrow 1,a}$, $LL_{0 \rightarrow 1,b}$ and $LL_{-1 \rightarrow 0}$ transitions increase with magnetic field (Fig. 3d and 3e). This is in a qualitative agreement with an increase of the number of states within each LL with magnetic field^{9,34}. However, a closer look at the absolute values of the spectral weights reveals a strong reduction with respect to the theoretical expectation for ideal graphene monolayers, as discussed in Section IV.

The scattering rate of the LL transitions is about 3 to 4 meV and magnetic field independent (Fig. 3f and 3h). Although in the case of the cyclotron peak we extracted the mobility using the scattering rate and the cyclotron frequency, in the quantum limit where the transition energy is proportional to \sqrt{B} , the quasi-classical Eq. (12) will formally result in diverging mobility values at low fields.

C. Temperature dependence

The temperature dependence of $\sigma_{xx}(\omega)$ and $\sigma_{xy}(\omega)$ at a fixed field of 3 T is shown in Fig. 4a and 4b, respectively. In both sets of curves, the CR structure changes weakly with temperature. The situation is different for the LL transitions. In $\sigma_{xx}(\omega)$ the LLs are preserved at all temperatures, although at elevated temperatures the peaks are about 3 meV broader than at low temperatures as obtained from the fits shown in the same graphs. Their spectral weight is almost temperature independent. However, in $\sigma_{xy}(\omega)$, the spectral features corresponding to the LL transitions are strongly diminished at high temperatures and almost disappear at room temperature.

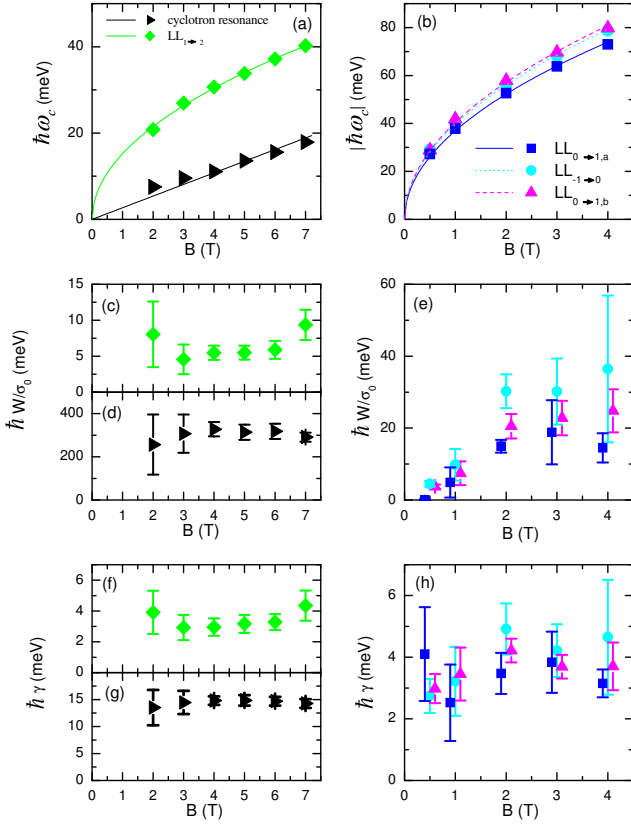


FIG. 3. Parameters of various components as a function of magnetic field obtained from the multi-component fits to $\sigma_{xx}(\omega)$ and $\sigma_{xy}(\omega)$ of Fig.2. (a) The transition energies of the CR (triangles) and the $LL_{1 \rightarrow 2}$ transition (diamonds). The solid lines are fits using Eq. (10) and Eq. (1) respectively. (b) The transition energies of $LL_{0 \rightarrow 1, a}$ (squares), $LL_{0 \rightarrow 1, b}$ (triangles) and $LL_{-1 \rightarrow 0}$ (circles) transitions. The solid lines are fits using Eq. (1). (c) Spectral weight of the $LL_{1 \rightarrow 2}$ transition. (d) Spectral weight of the CR peak. (e) Spectral weights of the $LL_{0 \rightarrow 1, a}$, $LL_{0 \rightarrow 1, b}$ and the $LL_{-1 \rightarrow 0}$ transitions. (f) The broadening of the $LL_{1 \rightarrow 2}$ transition. (g) The broadening of the CR transition. (h) The broadening of $LL_{0 \rightarrow 1, a}$, $LL_{0 \rightarrow 1, b}$ and the $-1 \rightarrow 0$ transitions. Errorbars in all figures are the standard deviation of several fitting results. The error bars in panels (a) and (b) are within the symbol size.

The extinction of the spectral structures corresponding to the LL transitions in $\sigma_{xy}(\omega)$ with warming up is due to the simultaneous presence of electron and hole like LL transitions as seen in the graphs of $\sigma_+(\omega)$ and $\sigma_-(\omega)$, plotted in Fig. 4c and 4d. At high temperatures, the electron- and hole- like components that have slightly different Fermi velocities overlap more, due to the increased broadening. In $\sigma_{xy}(\omega)$ the contributions are subtractive and more overlap results in weaker spectral structures. On the other hand, in $\sigma_{xx}(\omega)$, which is insensitive to the sign of the charge carriers, the contributions are additive and the transition peak appears less affected.

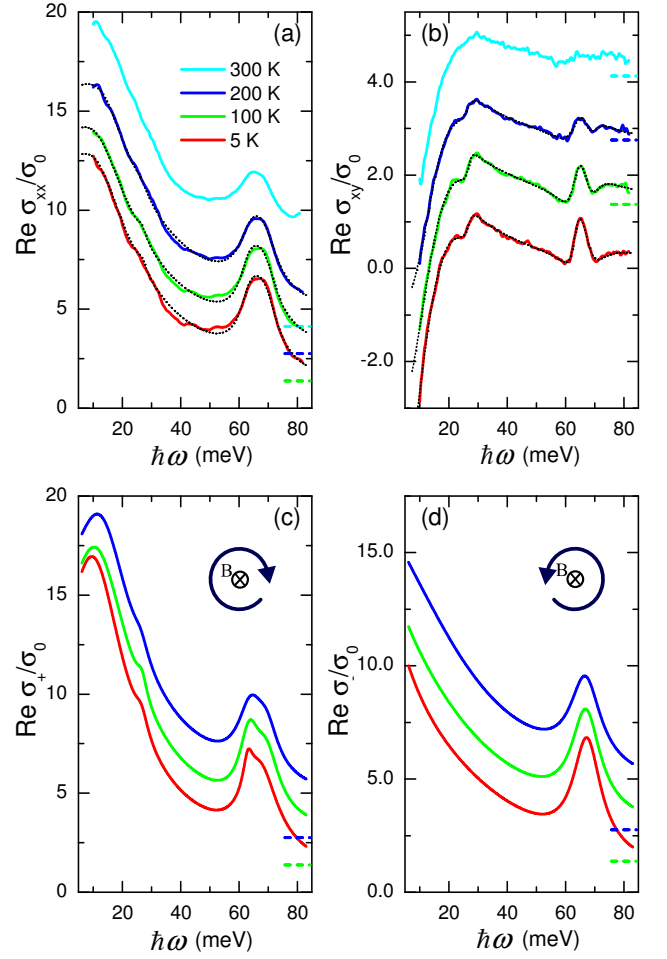


FIG. 4. Magneto-optical conductivity of multilayer graphene at 3 T, normalized to the universal conductivity σ_0 , for several temperatures between 5 K and 300 K. The curves in all panels are offset as indicated by the dashed lines. Larger offsets correspond to higher temperatures. Panels (a) and (b) show the measured spectra of $\sigma_{xx}(\omega)$ and $\sigma_{xy}(\omega)$ (solid lines) and multi-component fits (black dotted lines, only at 5, 100 and 200 K). In panels (c) and (d) the model-derived $\sigma_+(\omega)$ and $\sigma_-(\omega)$ are shown.

D. Effects of environmental doping

A careful inspection of the two series of measurements (Figs. 2 and 4) shows that the spectra from the different series taken at the same experimental conditions (5 K and 3 T) are not precisely the same, especially close to the $LL_{0 \rightarrow 1, a}$, $LL_{0 \rightarrow 1, b}$ and $LL_{-1 \rightarrow 0}$ transition energies. As was mentioned above, between these measurements the sample was held in dry air, therefore it is reasonable to assume that the difference is due to the effect of the environmental molecular contamination³⁵. In the case of multilayer graphene, the electronic properties of the outmost layer are most strongly modified, although one cannot exclude a certain effect on inner layers as well.

Fig. 5a shows the contributions of the $LL_{0 \rightarrow 1, a}$ and

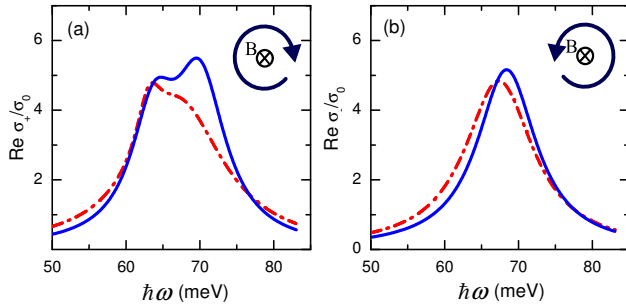


FIG. 5. The effect of environmental doping on the LL transitions at $B = 3$ T and $T = 5$ K. Panel (a): the contributions of the $LL_{0 \rightarrow 1,a}$ and $LL_{0 \rightarrow 1,b}$ transitions to $\sigma_+(\omega)$. Panel (b): the contribution of the $LL_{-1 \rightarrow 0}$ transition to $\sigma_-(\omega)$. In both panels, the red dash-dotted lines correspond to the measurement series as a function of temperature at constant magnetic field (Fig. 4), while the blue solid lines correspond to the measurement series as a function of magnetic field at constant temperature (Fig. 2). The curves are derived from the multi-component fits of experimental data.

$LL_{0 \rightarrow 1,b}$ transitions to $\sigma_+(\omega)$, for both measurements at 5 K and 3 T. The low energy $LL_{0 \rightarrow 1,a}$ transition with $v_F = 1.02 \times 10^6$ m/s is unaltered. The high energy $LL_{0 \rightarrow 1,b}$ transition with $v_F = 1.11 \times 10^6$ m/s however shows a clear change: the structure is much sharper in the second measurement. In Fig. 5b the contribution of the $LL_{-1 \rightarrow 0}$ transition to $\sigma_-(\omega)$ is plotted for both measurements. Similar to $LL_{0 \rightarrow 1,b}$, it shows a sharpening in the second measurement. The fact that both $LL_{0 \rightarrow 1,b}$ and $LL_{-1 \rightarrow 0}$ transition peaks are changed with environmental doping suggests that these transitions originate from the bands in the outmost graphene layer, which is most affected by surface contamination. The $LL_{0 \rightarrow 1,a}$ transition with the lowest v_F is unchanged by the environmental doping, therefore it probably comes from deeper graphene layers.

Fig. 3e shows that the spectral weights of the $LL_{0 \rightarrow 1,b}$ and $LL_{-1 \rightarrow 0}$ transitions are approximately equal, which indicates a balance between electrons and holes in the top layer. The Fermi velocity of the electrons (1.11×10^6 m/s) in that layer is slightly larger than the one of the holes (1.09×10^6 m/s). Similar results were found for monolayer exfoliated³³ and few layer CVD³⁶ graphene. The electron-hole asymmetry in our work (about 2%) is much smaller than the one found in Ref. 36, which might be due to different rotation angles between the layers in the used samples. Indeed, the asymmetry between electrons and holes was experimentally shown to depend on the relative rotation between subsequent graphene layers³⁶, where a large (small) rotation between the layers gives a small (large) asymmetry.

IV. DISCUSSION

Multilayer graphene on the C-side of SiC is often regarded as a stack of twisted monolayers, electronically de-

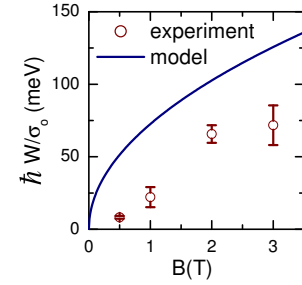


FIG. 6. Total spectral weight of the $LL_{0 \rightarrow 1,a}$, $LL_{0 \rightarrow 1,b}$ and $LL_{-1 \rightarrow 0}$ transitions (circles) as compared to the theoretical prediction for the spectral weight of the sum of the $LL_{0 \rightarrow 1}$ and $LL_{-1 \rightarrow 0}$ transitions in ideal monolayer graphene (solid line) with the chemical potential between E_{-1} and E_1 .

coupled from each other due to random rotational stacking, where the doping level varies across the layers due to the effects of the substrate and the surface contamination. Our observation of the CR and the LL transitions ($LL_{1 \rightarrow 2}$, $LL_{0 \rightarrow 1}$, $LL_{-1 \rightarrow 0}$) in the same spectra is a clear indication of this doping variation. Indeed, since only transitions between occupied and empty states can occur, their simultaneous activation implies different positions of the chemical potential with respect to the Dirac point energy. However, the activation of different LL transitions may also be caused by a spatial doping inhomogeneity.

The nearly perfect square-root dependence of the LL transition energies on magnetic field found in previous work^{9,26} and confirmed by the present measurements (Fig. 2a,b) is a signature of massless Dirac dispersion inherent to monolayer graphene. The same field dependence of LLs is obtained by STM^{10,11}. Accordingly, ARPES measurements¹² show multiple Dirac cones from individual layers. However, a number of our observations is difficult to fit into a simple picture of completely isolated monolayers. One of them is a significant (about 10%) spread of the Fermi velocity in the same sample. The largest values $v_F = 1.09 - 1.11 \times 10^6$ m/s we attribute to the outmost graphene layer, based on the effect of the surface contamination, while the smallest values, $v_F = 1.01 - 1.02 \times 10^6$ m/s, correspond to the inner layers, where the transitions $LL_{0 \rightarrow 1,a}$ and $LL_{1 \rightarrow 2}$ are active due to a weak electron doping. It was theoretically predicted^{16,18,19} that in rotationally stacked graphene layers the effect of the interlayer interaction is to reduce the Fermi velocity with respect to its ‘bare’ value in monolayer graphene. The variation of v_F that we find can thus be attributed to the effect of layer twisting and a randomness of the rotation angles between various layers.

It is important to compare not only the energies but also the optical spectral weights W of the LL transitions with theoretical expectations^{24,34}. Experimentally, we obtain the weights from the multi-component spectra fitting, described in Section III A. Let us consider the spec-

tral weights of the $LL_{0 \rightarrow 1}$ and $LL_{-1 \rightarrow 0}$ transitions. Assuming that the chemical potential is between the first electron and hole LLs (E_{-1} and E_1), the total weight of these transitions in monolayer graphene is given, according to the Kubo formalism for non-interacting Dirac fermions, by the transition energy itself³⁴:

$$\hbar W/\sigma_0 = 2(E_1 - E_0) = 2\sqrt{2e\hbar v_F^2|B|} \quad (13)$$

This dependence on magnetic field for $v_F = 1.0 \times 10^6$ m/s is plotted in Fig. 6 as a solid line. The symbols show the sum of the experimental spectral weights of the $LL_{0 \rightarrow 1,a}$, $LL_{0 \rightarrow 1,b}$ and $LL_{-1 \rightarrow 0}$ transitions. The experimental points are clearly below the theoretical curve. From here it follows that even if only in one graphene layer the chemical potential is between E_{-1} and E_1 then the total spectral weight observed is about 2 times smaller than the theoretical expectation. In reality it is likely that the number of layers in the present sample that satisfy the condition for the chemical potential is larger, which would make the deviation even stronger.

A possibly related experimental observation is the presence of the optical absorption background found from the fitting results of the phenomenological cyclotron multi-component model. This component, with vanishing ω_c , has a substantial spectral weight spread over a broad frequency range. The existence of the background shows that a significant amount of the charge carriers in the graphene layers neither fall into well defined CR nor LL transitions and signals a departure from the isolated monolayer description. In terms of the optical sum rule, the missing spectral weight of the LL transitions is transferred to the background. An intriguing question is whether this transfer is caused by interlayer coupling or by many-body effects within individual layers, such as electron-electron and electron-phonon interactions.

One should notice that the mobility and density of carriers in epitaxial graphene show a large variation from sample to sample, even when they are prepared under similar conditions³⁰. This shows that the interlayer twist angle, which is at the moment difficult to control experimentally, is a crucial parameter affecting the electronic and therefore optical properties of epitaxial graphene.

V. CONCLUSIONS

Using magneto-optical infrared Hall spectroscopy, the charge dynamics in multilayer epitaxial graphene grown on the C-side of SiC was studied in magnetic fields up to 7 T. The diagonal and the Hall conductivities were

extracted from the absorption and the Faraday rotation spectra, respectively. The latter is sensitive to the sign of charge carriers that allowed us to distinguish electrons and hole like transitions. The mobility and charge density of electrons were found, which makes this technique a useful contactless characterization tool.

A general multi-component model, Eq. (7), provided excellent fits at each field to $\sigma_{xx}(\omega)$ and $\sigma_{xy}(\omega)$ simultaneously. This analysis revealed the coexistence of optical transitions between individual LLs with a square-root dependence of the transition energies on magnetic field as expected for isolated monolayer graphene and a quasi-classical CR showing a linear magnetic field dependence. This is a clear indication of the doping variation across the layers.

We find the simultaneous presence of at least two distinct peaks due to transitions between Landau levels 0 and 1 (electrons). The separation between these peaks corresponds to a difference between the Fermi velocities of about 10%. One more peak due to a transition between LLs -1 (holes) and 0 is observed. The effect of the surface contamination on the spectra tells that both electrons and holes are present in the top layer and that electrons have slightly higher Fermi velocity than the holes (by 2%). The variation of the Fermi velocity is probably related to random twisting angles between graphene layers.

The spectral weight of the LL transitions is shown to be significantly reduced with respect to the theoretical expectation for a stack of fully decoupled graphene monolayers, assuming the picture of non-interacting electrons within each layer. This missing spectral weight correlates with the presence of an unexpected broadband optical absorption, which is also inconsistent with this simplified theoretical model.

Although the transition energies of the LL transitions clearly follow the magnetic field dependence expected for isolated graphene, in order to come to a complete picture of the complex electronic structure of multilayer graphene we need to understand the variation of the Fermi velocity, the small optical spectral weight of the LL transition and the broad absorption background in relation to the twist angle of the layers. Therefore, a systematic study of samples where this angle is experimentally controlled, is required.

This work was supported by the Swiss National Science Foundation (SNSF) by the grants 200021-120347 and IZ73Z0-128026 (SCOPES program), through the National Centre of Competence in Research Materials with Novel Electronic Properties-MaNEP. We thank S.G. Sharapov for useful discussions.

¹ C. Berger, Z. Song, T. Li, X. Li, A. Y. Ogbazghi, R. Feng, Z. Dai, A. N. Marchenkov, E. H. Conrad, P. N. First, and

W. A. de Heer, J. Phys. Chem. B, **108**, 19912 (2004).

² C. Berger, Z. Song, X. Li, X. Wu, N. Brown, c. Naud, D.

- Mayou, T. Li, J. Hass, A. N. Marchenkov, E. H. Conrad, P. N. First, and W. A. de Heer, *Science*, **312**, 1191 (2006).
- ³ K.V. Emtsev, A. Bostwick, K. Horn, J. Jobst, G. L. Kellogg, L. Ley, J. L. McChesney, T. Ohta, S. A. Reshanov, J. Röhrl, E. Rotenberg, A. K. Schmid, D. Waldmann, H. B. Weber, and Th. Seyller, *Nature Mater.* **8**, 203 (2009).
 - ⁴ A. Tzalenchuk, S. Lara-Avila, A. Kalaboukhov, S. Paolillo, M. Syväjärvi, R. Yakimova, O. Kazakova, T. J. B. M. Janssen, V. Fal'ko, and S. Kubatkin, *Nature Nano.* **5**, 186 (2010).
 - ⁵ C. Riedl, C. Coletti, T. Iwasaki, A.A. Zakharov, and U. Starke, *Phys. Rev. Lett.* **103**, 246804 (2009).
 - ⁶ F. Speck, M. Ostler, J. Röhrl, J. Jobst, D. Waldmann, M. Hundhausen, L. Ley, H. B. Weber, and Th. Seyller, *Mat. Sci. Forum* **645**, 629-632 (2010).
 - ⁷ P. N. First, W. A. de Heer, Th. Seyller, C. Berger, J. A. Stroscio, and J.-S. Moon, *MRS Bull.*, **35**, 296 (2010).
 - ⁸ J. Hass, F. Varchon, J. E. Millán-Otoya, M. Sprinkle, N. Sharma, W. A. de Heer, C. Berger, P. N. First, L. Magaud, and E. H. Conrad, *Phys. Rev. Lett.* **100**, 125504 (2008).
 - ⁹ M.L. Sadowski, G. Martinez, M. Potemski, C. Berger, and W. A. de Heer, *Phys. Rev. Lett.* **97**, 266405 (2006).
 - ¹⁰ D. L. Miller, K. D. Kubista, G. M. Rutter, M. Ruan, W. A. de Heer, P. N. First, and J. A. Stroscio, *Science* **324**, 924 (2009).
 - ¹¹ Y. J. Song, A. F. Otte, Y. Kuk, Y. Hu, D. B. Torrance, P. N. First, W. A. de Heer, H. Min, S. Adam, M. D. Stiles, A. H. MacDonald, and J. A. Stroscio, *Nature* **467**, 185 (2010).
 - ¹² M. Sprinkle, D. Siegel, Y. Hu, J. Hicks, A. Tejada, A. Taleb-Ibrahimi, P. Le Fèvre, F. Bertran, S. Vizzini, H. Enriquez, S. Chiang, P. Soukiassian, C. Berger, W. A. de Heer, A. Lanzara, and E. H. Conrad, *Phys. Rev. Lett.* **103**, 226803 (2009).
 - ¹³ X. Wu, Y. Hu, M. Ruan, N. K. Madiomanana, J. Hankinson, M. Sprinkle, C. Berger, and W. A. de Heer, *Appl. Phys. Lett.* **95**, 223108 (2009).
 - ¹⁴ F. Guinea, A. H. Castro Neto, and N. M. R. Peres, *Phys. Rev. B* **73**, 245426 (2006).
 - ¹⁵ E. McCann and V. I. Fal'ko, *Phys. Rev. Lett.* **96**, 086805 (2006).
 - ¹⁶ J. M. B. Lopes dos Santos, N. M. R. Peres, and A. H. Castro Neto, *Phys. Rev. Lett.* **99**, 256802 (2007).
 - ¹⁷ S. Shallcross, S. Sharma, and O. A. Pankratov, *Phys. Rev. Lett.* **101**, 056803 (2008).
 - ¹⁸ G. T. de Laissardière, D. Mayou, and L. Magaud, *Nano Lett.* **10**, 804 (2010).
 - ¹⁹ S. Shallcross, S. Sharma, E. Kandelaki, and O. A. Pankratov, *Phys. Rev. B* **81**, 165105 (2010).
 - ²⁰ E. J. Mele, *Phys. Rev. B* **81**, 161405 (2010).
 - ²¹ R. Bistritzer and A. H. MacDonald, *Phys. Rev. B* **81**, 245412 (2010).
 - ²² R. Bistritzer and A. H. MacDonald, arXiv:1101.2606 (2011).
 - ²³ I. Crassee, J. Levallois, A. L. Walter, M. Ostler, A. Bostwick, E. Rotenberg, Th. Seyller, D. van der Marel, and A. B. Kuzmenko, *Nature Physics* **7**, 48-51 (2011).
 - ²⁴ D. S. L. Abergel and V. I. Fal'ko, *Phys. Rev. B* **75**, 155430 (2007).
 - ²⁵ V. P. Gusynin, S. G. Sharapov, and J. P. Carbotte, *J. Phys. Condens. Matter* **19**, 026222 (2007).
 - ²⁶ M. Orlita and M. Potemski, *Semicond. Sci. Technol.* **25**, 06001 (2010).
 - ²⁷ Note that also transitions between electron- and hole-like LLs are optically allowed. However, for the used magnetic fields, these transitions are beyond the experimental spectral range, except at 0.5 T, where rather weak contributions from $LL_{-1 \rightarrow 2}$ and $LL_{-2 \rightarrow 1}$ could be discerned.
 - ²⁸ T. Ando, Y. Zheng, and H. Suzuura, *J. Phys. Soc. Jpn.* **71**, 13181324 (2002).
 - ²⁹ V. P. Gusynin, S. G. Sharapov, and J. P. Carbotte, *New J. Phys.* **11**, 095013 (2009).
 - ³⁰ M. Y. Lin, C. Dimitrakopoulos, D. B. Farmer, S.-J. Han, Y. Wu, W. Zhu, D. K. Gaskill, J. L. Tedesco, R. L. Myers-Ward, C. R. Eddy, A. Grill, and P. Avouris, *Appl. Phys. Lett.* **97**, 112107 (2010).
 - ³¹ A. M. Witowski, M. Orlita, R. Stępniewski, A. Wymolek, J. M. Baranowski, W. Strupiński, C. Faugeras, G. Martinez, and M. Potemski, *Phys. Rev. B* **82**, 165305 (2010).
 - ³² Z. Jiang, E. A. Henriksen, L. C. Tung, Y.-J. Wang, M. E. Schwartz, M. Y. Han, P. Kim, and H. L. Stormer, *Phys. Rev. Lett.* **98**, 197403 (2007).
 - ³³ R. S. Deacon, K.-C. Chuang, R. J. Nicholas, K. S. Novoselov, and A. K. Geim, *Phys. Rev. B* **76**, 081406(R) (2007).
 - ³⁴ V. P. Gusynin, S. G. Sharapov, and J. P. Carbotte, *Phys. Rev. Lett.* **98**, 157402 (2007).
 - ³⁵ F. Schedin, A. K. Geim, S. V. Morozov, E. W. Hill, P. Blake, M. I. Katsnelson, and K. S. Novoselov, *Nature Mat.* **6**, 652-655 (2007).
 - ³⁶ A. Luican, G. Li, A. Reina, J. Kong, R. R. Nair, K. S. Novoselov, A. K. Geim, and E. Y. Andrei, *Phys. Rev. Lett.* **106**, 126802 (2011).